Supporting Information

Photonic Torque Microscopy of the Nonconservative Force Field for Optically Trapped Silicon Nanowires

A. Irrera,[†,#] A. Magazzù,[†,#] P. Artoni,[‡,@] S. H. Simpson,[¶] S. Hanna,[§] P. H. Jones,[‖] F. Priolo,[‡,⊥] P. G. Gucciardi,[†] and O. M. Maragò[*,†]

CNR-IPCF, Istituto per i Processi Chimico-Fisici, I-98158 Messina, Italy, MATIS CNR-IMM and Dipartimento di Fisica e Astronomia, Università di Catania, I-95123, Catania, Italy, Institute of Scientific Instruments of the CAS, v.v.i. Czech Academy of Sciences, 612 64 Brno, Czech Republic, H. H. Wills Physics Laboratory, University of Bristol, BS8 1TL Bristol, UK, Department of Physics and Astronomy, University College London, WC1E 6BT London, UK, and Scuola Superiore di Catania, Università di Catania, I-95123 Catania, Italy

E-mail: marago@ipcf.cnr.it

[*]To whom correspondence should be addressed
[†]CNR-IPCF
[‡]MATIS CNR-IMM and Università di Catania
[¶]ISI-CAS
[§]University of Bristol
[‖]UCL
[⊥]Scuola Superiore di Catania
[#]These authors contributed equally to the work.
[@]Current address: Center for Life Science, Boston Children's Hospital, Harvard Medical School, Boston, USA

S1 Silicon nanowires synthesis

Figure S1a shows a typical scanning electron microscopy (SEM) image in cross-section of a dense array of ultrathin silicon nanowires (SiNWs), having a length of about 2 μm. This is obtained by using a field emission Zeiss Supra 25 scanning electron microscope. The SiNWs are synthesized by using metal-assisted wet etching of Si wafers. The process is schematically illustrated in fig. S1b. First, we evaporate a thin Au film on the silicon substrate with a thickness of 2 nm. This film exhibits a peculiar mesh-like morphology which leaves uncovered a relevant fraction of the Si surface.[1] Then we employ a HF+H_2O_2 aqueous solution for wet etching. The thin metallic mesh injects holes into the underlying Si. In regions where metal and Si are in contact, due to the presence of H_2O_2, Si oxidation occurs and the formed SiO_2 is removed by HF, producing the sinking of the metal into Si, and hence SiNW formation. At the end of the process metal particles remain trapped at the bottom of the etched regions, and they can be effectively removed by a selective etching process, so that no SiNW contamination occurs. We have indeed been able to define a very narrow thickness range of the metal films for which the layer morphology is able to determine the formation of SiNWs having an extremely small diameter.[2,3]

To synthesize the SiNW samples for our experiments, p-type (B concentration of 10^{16} cm^{-3}), single crystal, (100)-oriented Si wafers were cut into 1 cm$\times$1 cm pieces, and then UV oxidized and dipped in 5% HF to obtain clean and oxide-free Si surfaces. Afterwards, a thin Au layer, having a thickness of 2 nm (corresponding to 1.0×10^{16} Au atoms cm^{-2}), was deposited on the Si samples at room temperature by electron beam evaporation (EBE) by using high purity (99.99%) Au pellets as a source. The film thickness was determined by Rutherford backscattering spectrometry measurements. The metal-covered Si samples were etched at room temperature in an aqueous solution of HF (5 M) and H_2O_2 (0.44 M) to form SiNWs. Nanowire length was varied in the $1 - 5$ μm range, depending on the etching time, while the circular cross-section was measured to be constant and about 10 ± 2 nm from Raman and TEM analysis.[1,2] Finally, the removal of the Au was carried out by dipping

the sample in a KI + I_2 aqueous solution. The whole process works at room temperature. The process is maskless, cheap, fast and compatible with Si technology, so that it could be employed also for applications of Si nanostructures in an industrial environment.

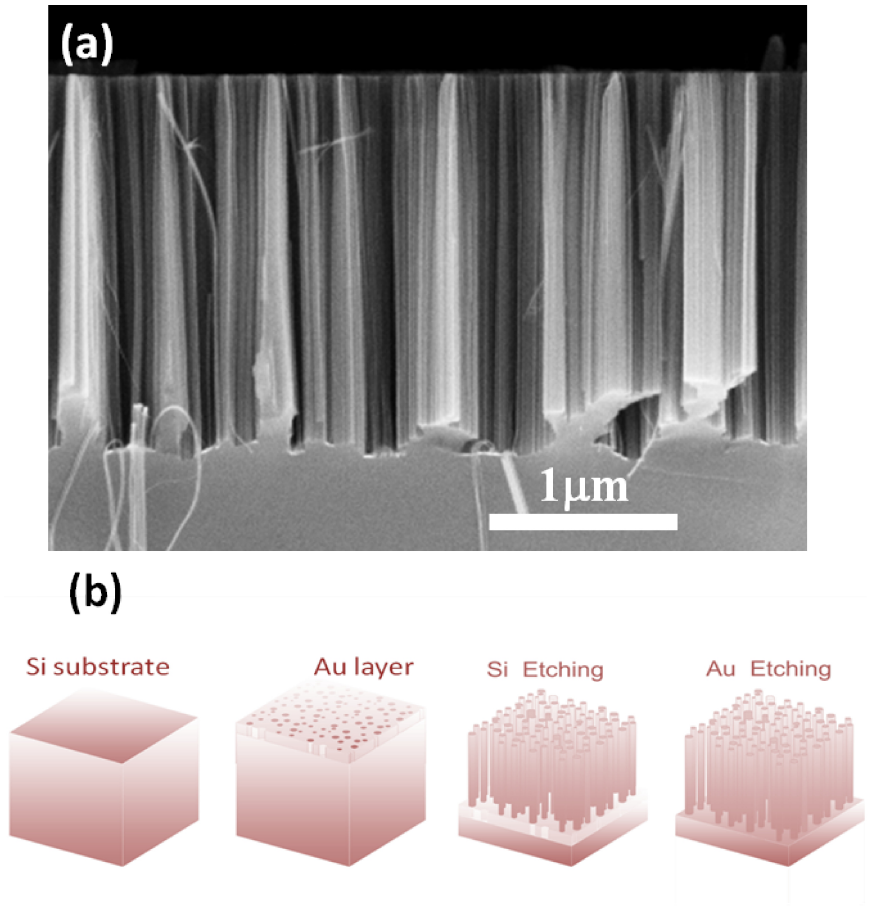

Figure S1: (a) Cross section SEM image of SiNWs on substrate as prepared. (b) Different stages of the preparation process of SiNWs on substrate. A silicon substrate is covered with a thin (2 nm) gold layer. The metal-covered silicon is etched at room temperature in an aqueous solution of HF to form SiNWs. Finally, gold is removed by dipping the sample in a KI + I_2 aqueous solution.

S2 Photonic torque microscopy and differential cross-correlations functions

We characterize the two-dimensional orbital motion of a silicon nanowire by photonic torque microscopy,[4,5] i.e., by studying the differential cross correlations functions (DCCFs) of the tracking signals obtained from the QPD. These DCCFs highlight the non-conservative orbital rotations and toroidal bias of a particle fluctuations in the optical trap.[6]

We consider the transverse motion of the SiNW in the x-y plane with the geometry depicted in fig. 1a of the main text. The motion resulting by the combination of the conservative trapping potential and the non-conservative contribution, $\epsilon_{xy} = \Omega_{xy}/\omega_\rho$, can be described by two coupled Langevin equation:[5,6]

$$\begin{cases} \dot{x}(t) &= -\omega_x x(t) + \epsilon_{xy}\omega_x y(t) + \sqrt{2D_\perp}\xi_x(t) \\ \dot{y}(t) &= -\epsilon_{xy}\omega_x x(t) - \omega_y y(t) + \sqrt{2D_\perp}\xi_y(t), \end{cases} \tag{1}$$

where $\omega_x = k_x/\gamma_\perp, \omega_y = k_y/\gamma_\perp$ are the trap relaxation frequencies controlling the decay of the autocorrelation functions,[7,8] $D_\perp = k_\mathrm{B}T/\gamma_\perp$ is the SiNW diffusion coefficient in the transverse plane, and $\xi_x(t), \xi_y(t)$ are uncorrelated white noise terms with unitary variance and zero mean. Assuming a small non-conservative contribution, $\epsilon_{xy} \ll 1$, the autocorrelation functions of the SiNW displacements do not depend on the non-conservative force and they assume the standard exponential form[7,8] typical of an overdamped regime. Instead, to reveal the non-conservative effects, in our analysis we consider the normalized differential cross-correlations (DCCFs) defined as:

$$DCCF_{xy}(\tau) = CCF_{xy}(\tau) - CCF_{yx}(\tau), \tag{2}$$

where $CCF_{xy}(\tau) = \langle x(t)y(t+\tau)\rangle / \sqrt{\langle x^2(t)\rangle\langle y^2(t)\rangle}$ represents the normalized cross-correlation between the x and y displacements as a function of lag time, τ, and $\langle x^2\rangle = D_\perp/\omega_x, \langle y^2\rangle = D_\perp/\omega_y$ are the mean-squared-displacements of the SiNW in the transverse plane. The expression of the DCCF is obtained following the work by Volpe *et al.*,[5] i.e., solving the coupled Langevin equation in a rotated frame in terms of the parameters $\omega_\rho = (\omega_x + \omega_y)/2$, $\Delta\omega = (\omega_x - \omega_y)/2$, and Ω_{xy}:

$$DCCF_{xy}(\tau) = \frac{2\sqrt{\omega_\rho^2 - \Delta\omega^2}}{\omega_\rho} e^{-\omega_\rho|\tau|} \, \frac{\Omega_{xy}}{\omega_\rho}\mathcal{S}(\tau) \tag{3}$$

where the expression of $\mathcal{S}(\tau)$ depends on the relative strength of the rotational field with respect to the confinement:[5]

$$\mathcal{S}(\tau) = \begin{cases} \omega_\rho \frac{\sin\left(\sqrt{|\Omega_{xy}^2 - \Delta\omega^2|}\tau\right)}{\sqrt{|\Omega_{xy}^2 - \Delta\omega^2|}}, & \Omega^2 > \Delta\omega^2 \\ \omega_\rho \tau, & \Omega^2 = \Delta\omega^2 \\ \omega_\rho \frac{\sinh\left(\sqrt{|\Omega_{xy}^2 - \Delta\omega^2|}\tau\right)}{\sqrt{|\Omega_{xy}^2 - \Delta\omega^2|}}, & \Omega_{xy}^2 < \Delta\omega^2 \ . \end{cases} \tag{4}$$

Thus, for the transverse DCCFs (shown in Figs. 2 and 3 of the main text) related to the SiNW motion in the x-y plane, we use the sinusoidal solution as fitting function of the observed DCCF_{xy} oscillations:

$$DCCF_{xy}(\tau) = \frac{2\sqrt{\omega_\rho^2 - \Delta\omega^2}}{\sqrt{|\Omega_{xy}^2 - \Delta\omega^2|}} e^{-\omega_\rho|\tau|} \ \frac{\Omega_{xy}}{\omega_\rho} \sin\left(\sqrt{|\Omega_{xy}^2 - \Delta\omega^2|}\tau\right), \tag{5}$$

and from the fit we obtain the non-conservative rotation frequency, Ω_{xy}.

Instead, for the ρ-z signals shown in Fig. S2a,b the non-conservative rotation is overdamped and hence we use the hyperbolic solution to fit the DCCFs and extract the rotation frequency, $\Omega_{\rho z}$:

$$DCCF_{\rho z}(\tau) = \frac{2\sqrt{\bar{\omega}^2 - \Delta\bar{\omega}^2}}{\sqrt{|\Omega_{\rho z}^2 - \Delta\bar{\omega}^2|}} e^{-\bar{\omega}|\tau|} \ \frac{\Omega_{\rho z}}{\bar{\omega}} \sinh\left(\sqrt{|\Omega_{\rho z}^2 - \Delta\bar{\omega}^2|}\tau\right), \tag{6}$$

where $\bar{\omega} = (\omega_\rho + \omega_z)/2$ and $\Delta\bar{\omega} = (\omega_\rho - \omega_z)/2$.

We find that the rotational contribution prevails in the x-y motion with rotational frequency Ω_{xy}, while thermal positional fluctuations overdamp the motion in the ρ-z plane. This latter situation is the same scenario that occurs for the non-conservative effects ob-

served for spherical particles,[6,9–11] i.e., an overdamped rotational bias resulting from the inhomogeneous longitudinal radiation pressure created by the highly focused laser beam. In Fig. S2b we also observe additional oscillations that are consistent with a fast center-of-mass motion in the axial direction driven by the non-conservative radiation forces, that testifies the richness and complexity of the system. Figures S2c and d show the scaling behavior of the non-conservative component, $\epsilon_{\rho z}$, as a function of power (Fig. S2c) and length (Fig. S2d). As for the transverse case, the behavior with length follows a L^{-1} scaling law.

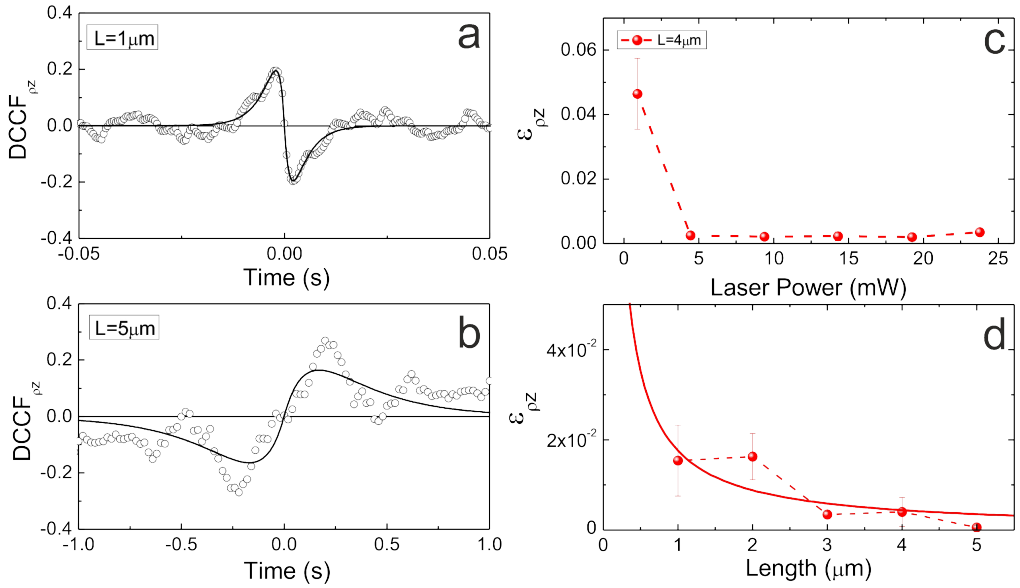

Figure S2: DCCFs in the ρ-z plane for two different SiNWs trapped at $P \sim 19$ mW with length $L \approx 1$ μm, in (a), and $L \approx 5$ μm, in (b). The DCCFs show an overdamped regime described by hyperbolic sinusoidal function as for the case of spherical particles. In (b) we also observe additional oscillations that are consistent with a fast center-of-mass motion in the axial direction. Non-conservative ρ-z component of the force field as function of optical trapping power (c) and SiNWs length (d). The red solid line is an hyperbolic fit representing a L^{-1} size scaling behavior.

S3 DCCF and circulation

The slope of the DCCF$_{xy}$ at $\tau = 0$ is related to the sense of the orbital rotation of the trapped SiNW. A positive slope is related to a counterclockwise (CCW) circulation of the Brownian vortex associated to a positive torque and work of the non-conservative force,

while a negative slope is related to a clockwise (CW) circulation and a negative torque and work. By breaking the tracks and calculating the DCCFs in subsequent intervals, we were able to observe in a few cases a reversal of the sense of rotation, i.e., a reversal of the DCCFs oscillations. This is shown in Fig. S3 where the DCCF_{xy} for a SiNW with length $L \sim 5$ μm. This confirms that the observed centre-of-mass orbital rotation depends on the orientational degrees of freedom that have a much longer relaxation time with respect to the translational ones.[7,8]

S4 Stochastic circulation induced by transverse polarization forces

Two factors are required to produce stochastic cycling of the sort observed in our experiments. First, the optical forces should be non-conservative, second they should induce a bias in the motion. The first of these conditions is satisfied almost everywhere in an optical tweezers. For example, even for a spherical particle in a standard optical trap, the curl of the force, $\nabla \times \mathbf{F}$, vanishes only at the trapping point.[6,9–11] In the vertical plane, including the beam axis, conservative gradient forces combine with scattering forces to induce a toroidal flux in the motion of weakly trapped spheres.[9,10] In the plane perpendicular to the optical axis, radiation forces on spheres are also non-conservative. Here, the conservative gradient forces are combined by non-conservative, inhomogeneous radiation pressure and transverse polarization forces that appear when the direction of polarization is oblique to the intensity gradient.[12,13] In Bliokh et al.[12] these forces are attributed to the imaginary Poynting vector related to the local spin density,[14] and referred to as the χ forces, where χ is the Stokes parameter measuring the degree of oblique polarization.[15] One expression of these χ forces in optical tweezers, would be the curvature of the lines of force seen for spheres displaced diagonally with respect to the polarization.[11,13] In the case of a sphere in a standard OT, the symmetry of the physical system means that there is no particular bias in the plane transverse to the optical axis (x-y plane). In particular, the orbital torque ($\mathbf{r} \times \mathbf{F}$) along the optical z-axis, experienced by a spherical particle following a stochastic fluctuation is as

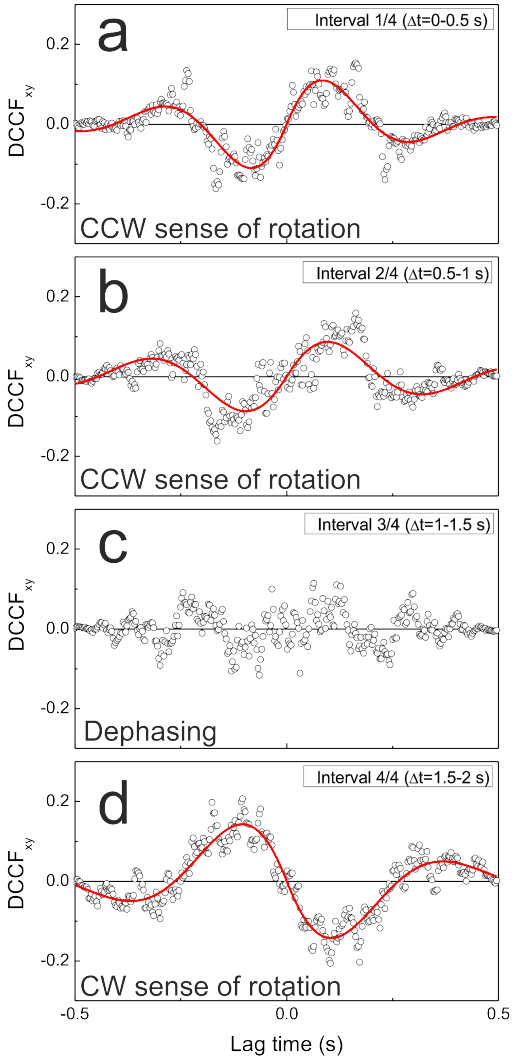

Figure S3: DCCF_{xy} obtained from 4 successive temporal intervals (0.5 s each) of the a SiNW tracking signal. In the first two intervals (a,b) the sense of rotation is positive and the circulation is CCW. In the third interval (c) the thermal fluctuations dephase the rotational bias and the DCCF oscillations. Thus, it is not possible to fit the DCCF with a sinusoidal function. In the last interval (d) the sense of rotation is reversed and the circulation is CW.

likely to be positive as negative, and on average it is zero.

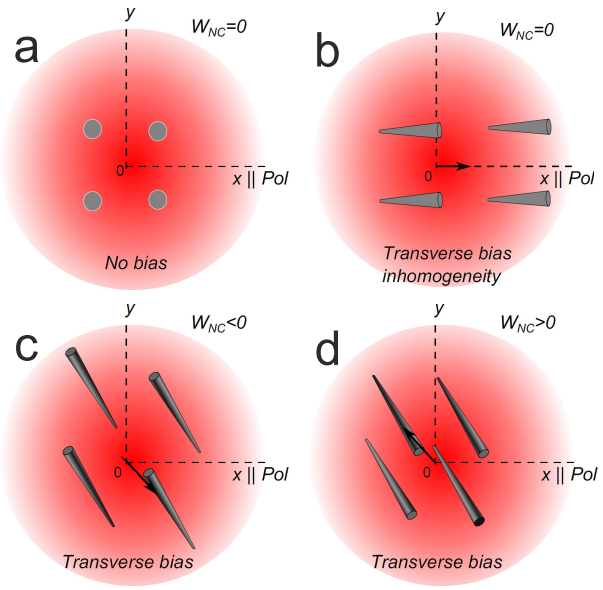

Figure S4: Schematic showing the symmetry of a system comprising a perfect Gaussian beam, polarized parallel to the x direction, for instance, and a particle displaced into each quadrant. (a) Symmetry requires that the force field for a spherical particle has inversion symmetry in the xy plane - suppressing a bias in the non-conservative force field. This holds true also for a nanowire aligned with the optical axis. (b) A nanowire tilted in the polarization direction generates a symmetric force field where, once again, there is no rotational bias. The bottom panels (c,d) show the symmetry when the nanowire is tilted obliquely. Mirror symmetry and inversion symmetry are broken, resulting in a bias that drives the thermal motion in a particular sense and consequently generate work.

In contrast to this, our experiments show a biased, stochastic cycling in the x-y plane. It is already known that optical forces in this plane are non-conservative,[11,13] due to the presence of transverse polarization forces. Driving this process requires a further breaking of symmetry, to bias the thermal motion and this is provided by the transverse radiation pressure induced by the non-spherical shape of the nanowire (Fig. S4). Experiments show that the sense of cycling varies from measurement to measurement, and that it can also change over the course of a measurement (Fig. S3). This indicates that the bias does not come from intrinsic properties of the beam or the wire. A candidate mechanism involves a systematic misalignment of the nanowire that persists throughout an observation. Such a scenario could arise, for example, as the nanowire is initially pulled into the beam.

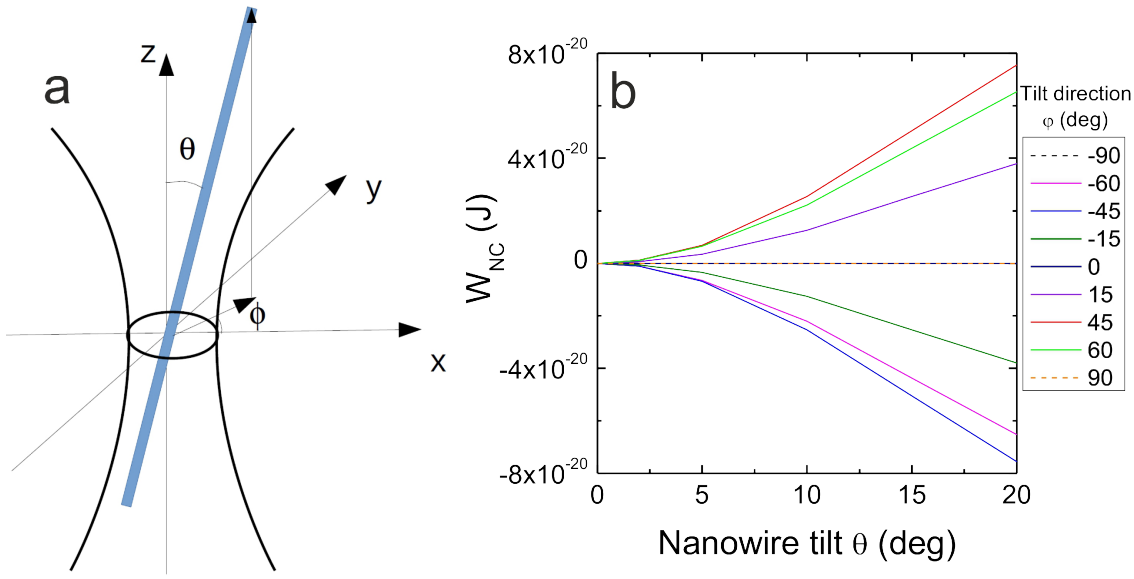

Figure S5: (a) Schematic showing the coordinates used in the simulations. (b) Work done on tilted nanowires as they are translated around a closed path in the x-y plane and for different tilt orientation, ϕ.

Here, we test this hypothesis with simulations of the forces on a 4 μm silicon nanowire, calculated with the coupled dipole method.[16] The tilt of the wire is described by two angles, θ, the polar angle that the wire makes with the vertical axis, parallel to the beam axis, and ϕ the azimuthal angle that the projection of the wire onto the x-y plane makes with the x axis (Fig. S5). The beam is polarized in the x direction with a power of 20 mW. First we apply a particular tilt to the nanowire, next we calculate the work done $\mathcal{W} = \oint \mathbf{F} \cdot d\mathbf{r}$, as the wire is translated about a circular loop in the x-y plane, centered at the trapping point and with a radius equal to the measured transverse RMS displacement,[8] $\sqrt{\langle \rho^2 \rangle} \approx 6$ nm. Figure S5b shows the result of such calculations for tilted wires with varying degrees of inclination to the vertical, θ, and tilted in varying directions ϕ. The results show that $\mathcal{W} \approx \theta^2 \sin(2\phi)$, in accordance with the symmetry based argument depicted in Fig. S4. Consequently, a persistent tilt (θ) and tilt direction (ϕ) can account for the different senses of rotation observed in the experiment. Note that the average tilt is dependent on the nanowire length as it is fixed by a balance between the restoring conservative torque of the

OT and the non-conservative torque generated by the transverse radiation pressure force. Moreover, as the average tilt is persistent to a certain value, so it is for the tilt direction that is biased by the transverse radiation pressure force. In fact, this force shifts the centre-of-mass of the wire away from the optical axis in a direction related to the average tilt, so both the average tilt angle and average direction are persistent variables. As a consequence, the centre of the resulting Brownian vortex is not on the optical axis.

S5 Center-of-mass position and fluctuations

The nanowire center-of-mass position on the optical axis (z-direction) is determined by the nulling of all the forces acting on the nanowire, i.e., axial gradient force, scattering forces, and gravity. While it is difficult to obtain an absolute measurement of the center-of-mass position in the trap from QPD signals (as they are based on thermal fluctuations analysis rather than absolute position calibration), we performed accurate calculations based on the coupled-dipole method to confirm and give an estimate of this upward pushing. Figure

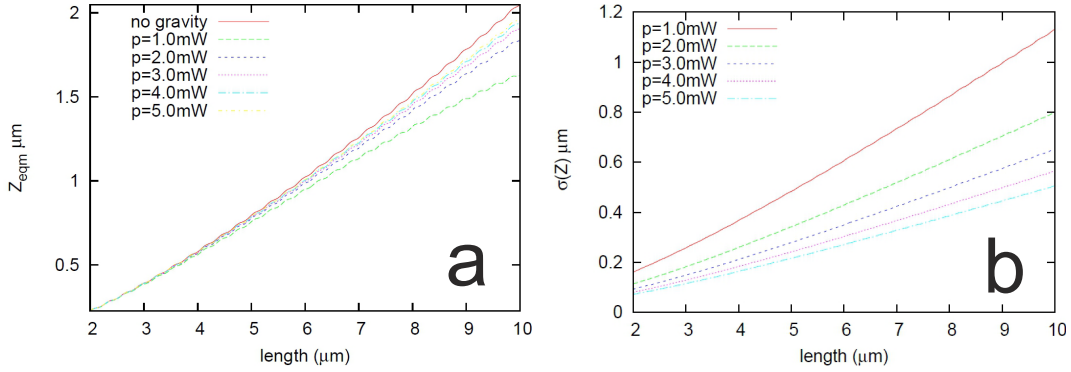

Figure S6: (a) Center-of-mass equilibrium position with respect to the focal point as a function of nanowire length for different incident power. (b) Axial positional fluctuations in the optical trap as a function of nanowire length at different laser power.

S6a shows the scaling with nanowire length of the center-of-mass equilibrium position with respect to the focal point for a silicon nanowire diameter of 50 nm and at different incident power. At variance with other experiments on thicker and longer nanowires,[17–19] our ultra-thin nanowires are pushed upwards with respect to the focal point only by about 10-20% of

their length by the longitudinal radiation pressure. Figure S6b compares the length scaling of the thermal fluctuations of the nanowire center-of-mass in the axial direction showing that they are decreasing consistently with power (as the trap gets stronger), and increasing with length as the trap becomes weaker for longer nanowires.[8,16] Note that this small amount of pushing is consistent with videomicroscopy images of ultra-thin optically trapped linear nanostructures such as silicon nanowires[8] and nanotubes[20] that show a change of phase in the images going from below to above the image plane demonstrating how these type of small diameter structures extend above and below the focal spot.

References

(1) Fazio, B.; Artoni, P.; Iati, M. A.; D'Andrea, C.; Lo Faro, M. J.; Del Sorbo, S.; Pirotta, S.; Gucciardi, P. G.; Musumeci, P.; Vasi, C.; Saija, R.; Galli, M.; Priolo, F.; Irrera, A. *Light: Science & Applications* **2016**, *5*, e16062.

(2) Irrera, A.; Artoni, P.; Iacona, F.; Pecora, E. F.; Franzo, G.; Galli, M.; Fazio, B.; Boninelli, S.; Priolo, F. *Nanotechnology* **2012**, *23*, 075204.

(3) Priolo, F.; Gregorkiewicz, T.; Galli, M.; Krauss, T. F. *Nat. Nanotechnol.* **2014**, *9*, 19–32.

(4) Volpe, G.; Petrov, D. *Phys. Rev. Lett.* **2006**, *97*, 210603.

(5) Volpe, G.; Volpe, G.; Petrov, D. *Phys. Rev. E* **2007**, *76*, 061118.

(6) Pesce, G.; Volpe, G.; De Luca, A. C.; Rusciano, G.; Volpe, G. *EPL (Europhysics Letters)* **2009**, *86*, 38002.

(7) Maragò, O. M.; Gucciardi, P. G.; Bonaccorso, F.; Calogero, G.; Scardaci, V.; Rozhinc, A. G.; Ferrari, A. C.; Jones, P. H.; Saija, R.; Borghese, F.; Denti, P.; Iatì, M. A. *Physica E: Low-dimensional Systems and Nanostructures* **2008**, *40*, 2347 – 2351.

(8) Irrera, A.; Artoni, P.; Saija, R.; Gucciardi, P. G.; Iatì, M. A.; Borghese, F.; Denti, P.; Iacona, F.; Priolo, F.; ; Maragò, O. M. *Nano Lett.* **2011**, *11*, 4879–4884.

(9) Roichman, Y.; Sun, B.; Stolarski, A.; Grier, D. G. *Phys. Rev. Lett.* **2008**, *101*, 128301.

(10) Sun, B.; Lin, J.; Darby, E.; Grosberg, A. Y.; Grier, D. G. *Phys. Rev. E* **2009**, *80*, 010401.

(11) Wu, P.; Huang, R.; Tischer, C.; Jonas, A.; Florin, E.-L. *Phys. Rev. Lett.* **2009**, *103*, 108101.

(12) Bliokh, K. Y.; Bekshaev, A. Y.; Nori, F. *Nat. Commun.* **2014**, *5*, 3300.

(13) Iglesias, I.; Sáenz, J. J. *Opt. Commun.* **2011**, *284*, 2430–2436.

(14) Albaladejo, S.; Marqués, M. I.; Laroche, M.; Sáenz, J. J. *Phys. Rev. Lett.* **2009**, *102*, 113602.

(15) Antognozzi, M.; Simpson, S.; Harniman, R.; Senior, J.; Hayward, R.; Hoerber, H.; Dennis, M. R.; Bekshaev, A. Y.; Bliokh, K. Y.; Nori, F. *Nature Physics* **2016**,

(16) Simpson, S.; Hanna, S. *Nanotechnology* **2012**, *23*, 205502.

(17) Pauzauskie, P. J.; Radenovic, A.; Trepagnier, E.; Shroff, H.; Yang, P.; Liphardt, J. *Nat. Mater.* **2006**, *5*, 97–101.

(18) Neves, A. A. R.; Camposeo, A.; Pagliara, S.; Saija, R.; Borghese, F.; Denti, P.; Iatì, M. A.; Cingolani, R.; Maragò, O. M.; ; Pisignano, D. *Opt. Express* **2010**, *18*, 822–830.

(19) Reece, P. J.; Toe, W. J.; Wang, F.; Paiman, S.; Gao, Q.; Tan, H. H.; Jagadish, C. *Nano Lett.* **2011**, *11*, 2375–2381.

(20) Maragò, O. M.; Jones, P. H.; Bonaccorso, F.; Scardaci, V.; Gucciardi, P. G.; Rozhin, A.; Ferrari, A. C. *Nano Lett.* **2008**, *8*, 3211–3216.